Development, Characterization, and Circuit Modeling of Inkjet-Printed Coupled Ring Resonators for Application in Biological Samples

Giovanni Gugliandolo, *Member, IEEE*, Giovanna Vermiglio, Giuseppina Cutroneo, Giuseppe Campobello, *Member, IEEE*, Giovanni Crupi, *Senior Member, IEEE*, and Nicola Donato, *Senior Member, IEEE*

***Abstract*— In the present study, the inkjet-printing (IJP) technique is used for the development of a planar microwave sensor aimed at the dielectric characterization of biological samples. The proposed sensor consists of two capacitively coupled split-ring resonators (SRRs) fabricated using the microstrip technology. A silver-based conductive ink is deposited by IJP on a conventional 1.6-mm-thick FR4 substrate, thus creating the resonant structure. The experimental analysis is carried out by considering a water–ethanol mixture as a test solution in which the ethanol volume fraction is varied, thereby changing the effective permittivity of the mixture. In this contribution, the authors focused their analysis on the dielectric constant of the solution under test (i.e., the real part of the complex relative permittivity). The water–ethanol mixture is placed into a low-density polyethylene (LDPE) sample vial that is arranged on the surface of the planar sensor. No direct contact is needed between the microwave device and the solution under test. The effect of the ethanol volume fraction change is related to the behavior of the two resonances occurring in the forward transmission coefficient (S_{21}) of the sensor in the frequency range from 2 to 3 GHz. The permittivity change of the sample under test affects the capacitive coupling between the two SRRs altering the separation between two resonant frequencies. This enables the sensor to differential measurements, thereby improving its robustness. The frequency separation is used to track variations in the ethanol concentration and, thus, the dielectric constant of the solution under test. In addition, a lumped-element equivalent-circuit model is presented, and the changes in the values of the lumped elements with ethanol concentration are estimated and discussed.**

***Index Terms*— Biological materials, equivalent circuits, inkjet printing (IJP), microwave sensors, scattering parameters, split-ring resonators (SRRs).**

I. Introduction

INKJET printing (IJP) is a powerful and rapidly increasing printing method that involves the ejection of ink droplets onto a rigid or flexible substrate [1]. This technology has been successfully used with a variety of substrates (e.g., paper, polyimide, polyethylene terephthalate, plastic, fiberglass, and ceramic) and different types of inks, including polymer, metal, and carbon [2], [3], [4]. Because of its many interesting qualities and high applicability for adoption in a wide range of applications, IJP stands out among the other competing technologies. Among others, IJP has the advantages of being a contactless (i.e., no physical contact between the printing equipment and the substrate) and mask-free process that allows for quick production times, cost-effectiveness, material savings, good reproducibility, and high spatial resolution [5]. Recently, IJP technology based on flexible substrates has attracted increasing attention due to its use in the production of flexible and wearable electronic devices [6], [7], widely used for healthcare applications [8]. Moreover, this technology represents a highly attractive solution for sensor development since it is applicable to large-scale production of cost-effective devices with an acceptable level of reproducibility [5], [9].

In the recent literature, several IJP-based devices have been proposed for sensing purposes, including sensors for gas, fluid, strain, pressure, temperature, and humidity measurements [10], [11], [12], [13], [14], [15], [16], [17], [18]. Furthermore, the IJP technology has been successfully applied for the characterization of biological samples, such as cell cultures [19], [20], [21], [22]. It is an attractive research field that is essential for the progress of the biomedical and pharmaceutical industries [23], [24], [25]. In such a context, the goal of this research is the development, characterization, and analysis of an inkjet-printed microwave resonator for application aimed at biological samples.

The prototype proposed in this study consists of two capacitive coupled split-ring resonators (SRRs). To the best of our knowledge, so far this type of geometry has not been used for differential measurements, which can significantly improve the sensing robustness [26]. As a matter of fact, possible variations in the surrounding environment are seen as a common mode effect that can be minimized by the differential detection mechanism of the device [27].

The prototype is fabricated by printing on an FR4 substrate a silver-based conductive ink. The employed ink is a commercial conductive ink characterized by a high oxidation resistance and a low electrical resistivity. The sensor is designed by means

Manuscript received 11 October 2022; revised 2 March 2023; accepted 1 April 2023. Date of publication 1 May 2023; date of current version 10 May 2023. The Associate Editor coordinating the review process was Dr. Tarikul Islam. *(Corresponding author: Giovanni Gugliandolo.)*

Giovanni Gugliandolo, Giuseppe Campobello, and Nicola Donato are with the Department of Engineering, University of Messina, 98166 Messina, Italy (e-mail: giovanni.gugliandolo@unime.it; gcampobello@unime.it; ndonato@unime.it).

Giovanna Vermiglio, Giuseppina Cutroneo, and Giovanni Crupi are with the Department of Biomedical and Dental Sciences and Morphofunctional Imaging, University of Messina, 98125 Messina, Italy (e-mail: giovanna.vermiglio1@unime.it; giuseppina.cutroneo@unime.it; crupig@unime.it).

Digital Object Identifier 10.1109/TIM.2023.3271010

of a professional computer-aided design (CAD) simulation tool, whereas the experimental validation is performed by measuring the scattering (S-) parameters with a vector network analyzer (VNA).

This study is an extension of our previous work [7] in which a microwave-coupled resonator was proposed for the dielectric characterization of cell cultures. The present study extends the previous findings by means of an extraction procedure based on a lumped-element equivalent-circuit model. This model allows us to describe the proposed device locally, specifically near its two resonances. The lumped-element equivalent-circuit model is an important tool for understanding the behavior of the sensor and its response to changes in the dielectric properties of the liquid under test. Furthermore, the extraction of the relative variation of the lumped-element values provides a thorough characterization of the sensor and its performance. This is crucial for the design and optimization of the sensor and for the development of new sensing applications. The microwave sensor is validated by considering a variable mixture of water and ethanol as a case study. The mixture is placed into a low-density polyethylene (LDPE) sample vial and arranged on the surface of the planar sensor for its characterization. This is carried out by relating the effect of the ethanol volume fraction change in the testing solution to the behavior of the two resonances occurring in the forward transmission coefficient (S_{21}) of the sensor in the frequency range from 2 to 3 GHz. It is worth noting that planar resonators have been widely employed for sensing purposes and have exhibited good performance when used in the frequency range between 1 and 3 GHz [23], [25], [28], [29]. The obtained results demonstrate the validity of the designed sensor and its possible application to the dielectric characterization of other types of materials. In a future perspective, the sensor performance will be evaluated considering different types of biological samples. Moreover, since the proposed device operates in the RF range, it may be possible to integrate it into an antenna for remote sensing applications [30].

The article is organized as follows: Section II is devoted to the description of the topology and working principle of the planar microwave resonator; Section III includes a description of the design and fabrication of the prototype sensor; Section IV deals with the extraction of the main resonant parameters from the acquired forward transmission coefficient; Section V is aimed at presenting the experimental characterization; and Section VI is focused on the analysis and discussion of the achieved results. Conclusive remarks are given in Section VII.

II. Coupled SRRs

This section is divided into two subsections. The first one is devoted to the introduction of the equivalent-circuit model topology of the studied sensor, whereas the second one is dedicated to the description of its operating principle.

A. Equivalent-Circuit Model

The microwave sensor employed in this work consists of two capacitively coupled SRRs designed in microstrip technology. The selected geometry is depicted in Fig. 1. Two 50-Ω microstrip lines are used as feedlines for the coupled resonator. By using the TXLINE tool of the AWR Design Environment 16 software, the nominal line impedance is estimated to vary only slightly over the whole explored frequency range (i.e., from 50.0 Ω at 2 GHz to 50.1 Ω at 3 GHz). This resonator structure has been already used in previous studies for sensing applications, and the achieved results showed good performance in terms of NaCl detection in water and ice [31], [32].

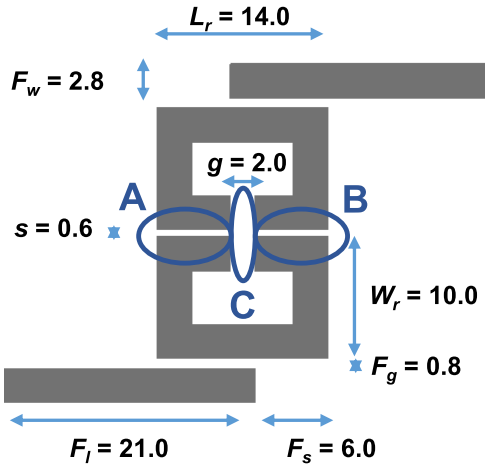

Fig. 1. Drawing of the top view of the two-port microwave sensor under study. All dimensions are in millimeters.

Each ring is characterized by a resonant frequency f_r that can be expressed as [31]

$$f_r = \frac{c}{2 \times l \times \sqrt{\varepsilon_{\text{eff}}}} \tag{1}$$

where c is the speed of light in the vacuum, l is the physical length of the ring, and ε_{eff} is the effective permittivity of the ambient nearby the microwave resonator. Since the two rings have the same geometry, they are supposed to resonate at the same frequency. However, the two rings are capacitively coupled, and this coupling leads to a frequency-splitting phenomenon. The splitting is tunable by changing the geometrical parameters of the resonators that affect the coupling factor between the two rings [31]. A lumped-element equivalent-circuit model for the selected microwave resonator is shown in Fig. 2. It is the same equivalent-circuit topology described in [33], which is here exploited for the lumped-element extraction procedure and the subsequent analysis. The elements L and C_r represent the self-inductance and self-capacitance, i.e., the equivalent inductance and capacitance exhibited by the uncoupled resonator. Without coupling, the resonator is characterized by a resonant frequency $f_r = 1/(2\pi\sqrt{LC_r})$. The mutual capacitance C_m represents the capacitive coupling effect [33]. The equivalent-circuit model depicted in Fig. 2 is characterized by two resonant frequencies [33]

$$f_L = \frac{1}{2\pi\sqrt{L(C_r + C_m)}} \tag{2}$$

$$f_H = \frac{1}{2\pi\sqrt{L(C_r - C_m)}}. \tag{3}$$

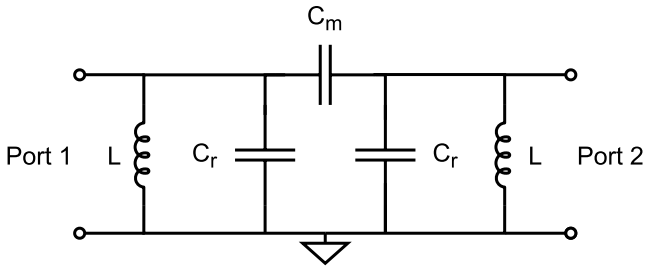

Fig. 2. Lumped-element equivalent-circuit model for the two-port resonator.

The resonant frequency f_L is lower in comparison with that of the uncoupled SRR. A physical interpretation of such behavior is that the coupling effect increases the ability of the resonator in charge storing. On the other hand, at f_H, the coupling effect limits this ability since f_H is higher in comparison with that of the uncoupled SRR [33].

B. Sensor Operating Principle

The two resonant frequencies of the coupled resonator depend on geometrical parameters as well as the dielectric properties of both the resonator materials and the ambient surrounding the resonator itself. Once the final design is selected and the resonator is fabricated on its substrate, the device is still affected by an alteration in the permittivity in the near ambient. This can be exploited for sensor development. In a planar microwave resonant sensor, a change in the dielectric properties of a surrounding material is transduced into an alteration in the electric field that results in a change in the resonant frequency [34], [35], [36], [37].

The working principle of the presented microwave sensor relies on the change in the dielectric properties of the ambient near the sensor itself. For instance, a variation of the dielectric constant ε_r of a medium surrounding the microwave device leads to an alteration in the features of the two resonances. This can be observed as a deviation of the main resonant parameters, i.e., the resonant frequency f_r and the quality (Q-) factor. Such deviations can be related to the ε_r of the medium under test so that, after a calibration procedure, it is possible to exploit f_r and Q to track the change in ε_r of the medium. Regions A, B, and C, which are shown in Fig. 1, are the most sensible regions of the sensor surface [31], [32]. In light of the information published in the literature [31], if a testing material is placed over the sensor surface in region A or B and its ε_r is varied, one resonance results to be more affected than the other one. In other words, a frequency shift is observed mainly in one resonance. On the other hand, if the testing material is placed above the sensor covering also the region C, both resonances are affected [32]. In the present study, the sample under test is placed in region B, as far as possible from central region C, thus making only one resonance sensible to the ε_r variation of the sample. This allows one to select one resonant frequency as reference (e.g., the less sensitive one) and consider the difference $f_{r_2} - f_{r_1}$ as a tracker for the sample ε_r changes. If a bias error affects both resonant frequencies, it will be minimized by considering their difference.

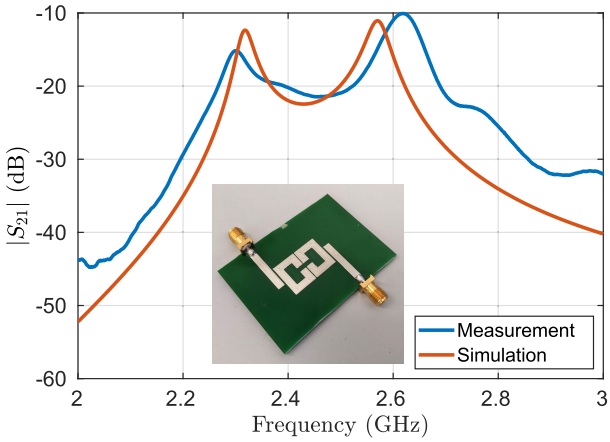

Fig. 3. Frequency-dependent behavior of the magnitude of the forward transmission coefficient for the developed sensor: measurements (blue line) and simulations (orange line). The selected frequency range is from 2 to 3 GHz with a step of 625 kHz. The inset shows a photograph of the top view of the developed two-port resonator. It is fabricated on a 1.6-mm-thick FR4 substrate. The overall board dimensions are 60 × 20 × 1.6 mm.

III. Sensor Design and Fabrication

The microwave device is intended to operate at frequencies ranging from 2 to 3 GHz. The sensor geometry has been selected in order to optimize both the peak amplitude and the Q-factor. In addition, the resonance frequency spacing (i.e., $f_{r_2} - f_{r_1}$) has been carefully selected: a large frequency separation will result in an increase in the device bandwidth, which is not an advantage in most cases; on the other hand, if the separation is too small, it will be difficult to distinguish between the two resonances, thus making the accurate evaluation of the resonant frequencies and the quality factors challenging. For the selected prototype, a frequency spacing of about 250 MHz is chosen as a good compromise. The sensor design has been performed using professional CAD software (AWR Design Environment 16). Once the design process is finalized, the sensor is fabricated using the IJP technique by means of the Voltera V-One printed circuit board (PCB) printing machine. As the device under test is an inkjet-printed sensor, the uniformity of the geometry is a major concern. The printing process may lead to imperfections if the inkjet printer is not set up properly, and the setup might depend on various factors, such as the resonator geometry, nozzle dimension, conductive ink used, and substrate. To ensure that the printing results are of the highest possible quality and that there is minimal nonuniformity in the resonator geometry, a calibration procedure is carried out before the printing process on a commercial FR4 substrate, by considering also its nonperfect planarity. This calibration procedure is used to set all the printer parameters properly. As shown in Fig. 3, a comparison between the simulated forward transmission coefficient and the measured one shows a good agreement, which serves as evidence of the effectiveness of the calibration procedure.

A silver-based conductive ink (Voltera Conductor 2, nominal resistivity $= 1.265 \times 10^{-7}\ \Omega \cdot \mathrm{m}$) is deposited by IJP on a 1.6-mm-thick FR4 substrate according to the sensor final geometry (see Fig. 1). On the opposite side of the substrate, a uniform layer of the silver-based conductive ink is

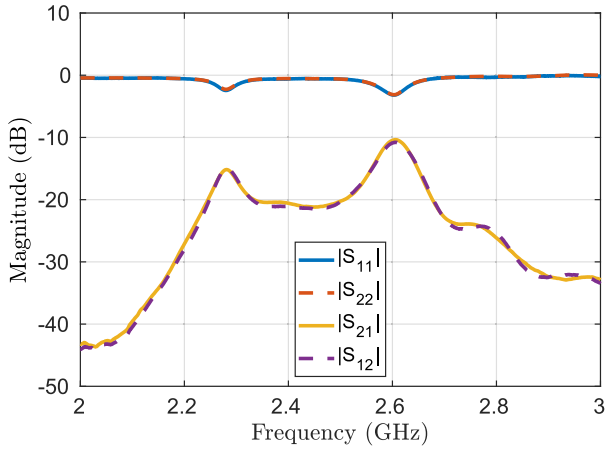

Fig. 4. Frequency-dependent behavior of the magnitude of the S-parameters. The device behaves in the first approximation as a symmetrical device (i.e., $S_{11} = S_{22}$ and $S_{21} = S_{12}$).

deposited in order to create the ground plane of the microstrip structure. The prototype is then cured in an oven at 200 °C for approximately 30 min. This step is essential for triggering the chemical processes in the conductive ink that will allow the metallic particles to combine and form the conductive layer. Next, the sensor is cleaned with isopropyl alcohol and burnished to remove any possible solvent residues or oxides. Finally, two SMA connectors are soldered at the end of the two 50-Ω feedlines for the VNA connection. A photograph of the top view of the fabricated sensor is shown in the inset of Fig. 3.

The sensor is connected to the VNA for the acquisition of the (S-) parameters in the frequency range from 2 to 3 GHz. As illustrated in Fig. 4, the microwave resonator behaves, in the first approximation, as a symmetrical device (i.e., $S_{11} = S_{22}$ and $S_{21} = S_{12}$). In the present study, the forward transmission coefficient (i.e., S_{21}) is considered for data analysis. Fig. 3 reports a comparison of the simulated and measured $|S_{21}|$. It is worth noting that, as expected, the two resonant peaks, which appear in the magnitude of the transmission coefficient, occur in both simulations and measurements. The frequency spacing appears wider in the measured data (320 MHz) than in the simulations (250 MHz). Furthermore, it is observed that the Q-factors of two resonances in the measurements are lower than those in the simulations, owing to a higher resistivity of the conductive ink compared with its nominal value used for the simulations. The experimental analysis of the device under test verified the presence of two resonant peaks at 2.30 and 2.62 GHz. These resonance frequencies are here denoted by the symbols f_L and f_H and are characterized by a Q-factor of 40 and 44, respectively.

IV. Extraction of the Resonant Parameters

The evaluation of the Q-factor and the resonant frequency from the two peaks is fulfilled by means of a double-Lorentzian curve fitting algorithm. The developed software is similar to that used in [38], [39], and [40]. The fitting software is written in Python using the *scikit-rf* package and the *lmfit* library. This software is able to read the touchstone files and extract the two Lorentzian curves from the acquired forward transmission coefficient by means of a curve-fitting method. In particular, among the various fitting methods allowed by the *lmfit* library, in this work, the Levenberg–Marquardt algorithm is selected since its performance fits well with the project requirements (i.e., $R^2 > 0.9$ with an execution time of about 60 ms for each fitting). The complex forward transmission coefficient, as a function of the frequency f, is modeled as the sum of two Lorentzian functions and a background signal

$$S_{21}(f) = L_1(f) + L_2(f) + B(f). \tag{4}$$

The Lorentzian functions $L_i(f)$ are two identical complex functions in the form

$$L_i(f) = \frac{a_i f}{f^2 - f_i^2} \tag{5}$$

where a_i and f_i are two complex coefficients. In particular, f_i can be expressed as

$$f_i = f_{r_i} + j g_i. \tag{6}$$

The real part f_{r_i} is the resonant frequency, whereas the imaginary part is used for the Q-factor estimation

$$Q_i = \frac{f_{r_i}}{2g_i}. \tag{7}$$

The function $B(f)$ represents the background signal, and it is a complex polynomial function of order N. In this case, $N = 2$ was enough for a good fitting

$$B(f) = \sum_{n=0}^{N} = 2b_n \left(f - f_{r_i}\right)^n \tag{8}$$

where b_n are complex coefficients.

The developed software draws out the two Lorentzian complex functions from the acquired S_{21} parameter and, for each Lorentzian function, the software returns the best estimation of the resonant frequency, the Q-factor, and the resonant-peak amplitude. The fitting process is essential in this case since the two resonant peaks in the magnitude of the transmission coefficient are coupled with each other, and their overlap may result in an inaccurate evaluation of the main resonant parameters (i.e., f_r and Q) [41]. The double-Lorentzian fitting is illustrated in Fig. 5. The red line is the acquired S_{21}, whereas the blue line is the fitting function. It is the result of a combined contribution of the two Lorentzian functions, depicted in Fig. 5 by dashed lines.

V. Measurements

For the sensor validation, a liquid testing mixture of water and ethanol is considered. The mixture is placed into an LDPE sample vial that is put above the sensor surface, as shown in Fig. 6. It is worth noting that the liquid mixture is not directly in contact with the microwave resonator.

The proposed sensor is tested toward the water/ethanol solution, and a parameter extraction procedure is applied for a better understanding of the device's performance. A schematic of the experimental workflow can be found in

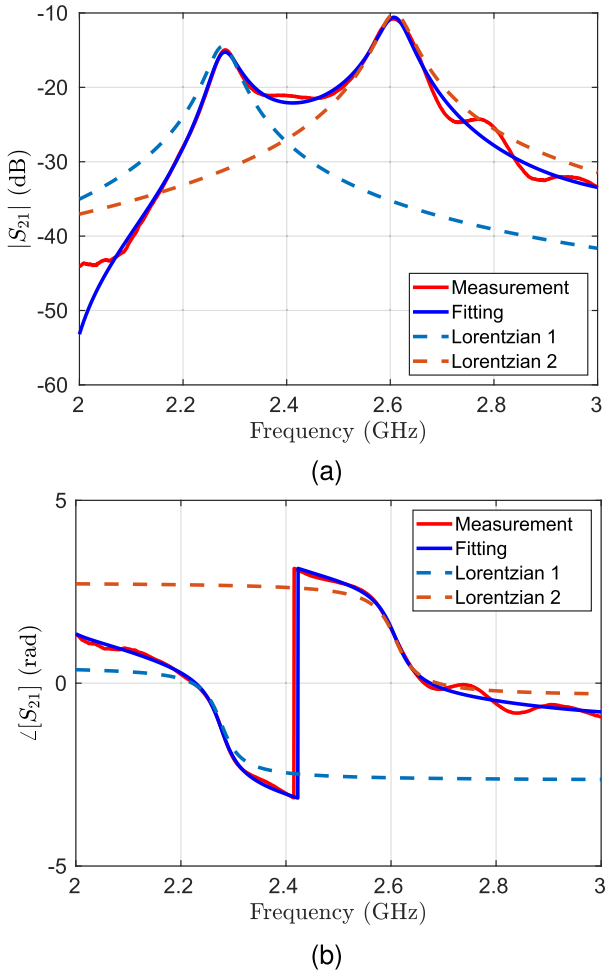

Fig. 5. Frequency-dependent behavior of the (a) magnitude and (b) phase of the forward transmission coefficient for the developed sensor: measurements (red solid line) and Lorentzian fitting (blue solid line). The fit function is obtained as the result of the combined contributions of the two Lorentzian functions (dashed lines).

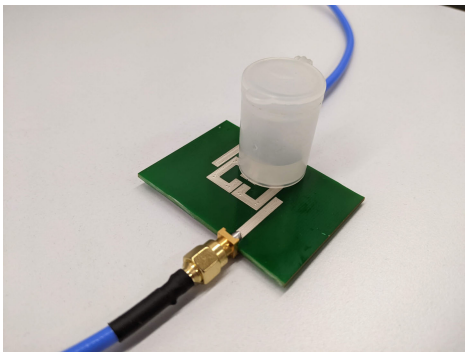

Fig. 6. Photograph of the LDPE sample vial containing the water–ethanol mixture placed over the microwave sensor. The solution volume is kept constant at 2 cm^3.

Fig. 7. The extraction procedure will be described in detail in Section VI.

The vial is filled with a variable mixture of ethanol ($\varepsilon_r = 25.16$ [42]) and pure water ($\varepsilon_r = 80.2$ [42]) at different volume ratios in five different steps. The vial diameter, height, and wall thickness are 22.8, 32.9, and 1.35 mm, respectively. Its total capacity is 7 mL. For each volume fraction, the mixture

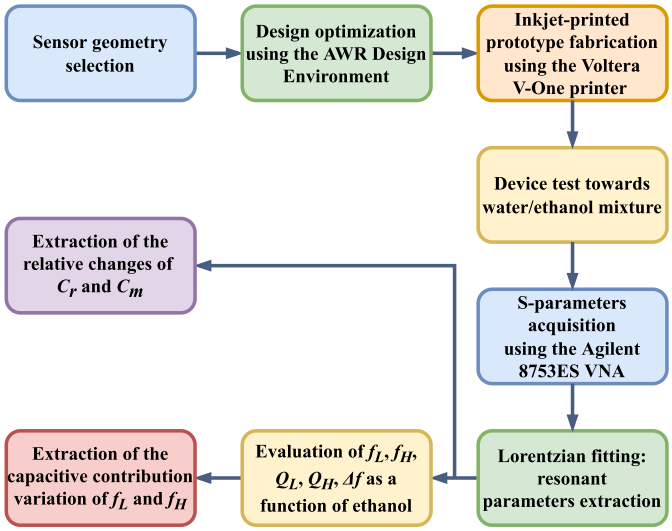

Fig. 7. Schematic of the experimental workflow: from the sensor design to the capacitive contribution extraction as a function of the ethanol volume fraction.

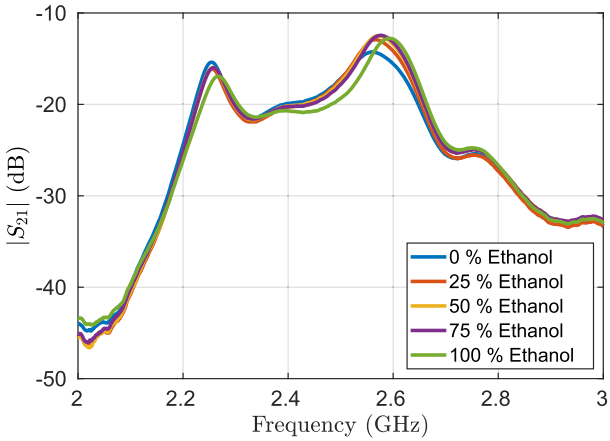

Fig. 8. Measurements of the magnitude of the forward transmission coefficient at five different ethanol concentrations in water. The selected frequency range is from 2 to 3 GHz with a step of 625 kHz.

exhibits a different ε_r, from 25.16 (pure ethanol) to 80.2 (pure water). This enabled the sensor to be tested on a relatively wide range of ε_r, compatible with the typical ε_r changes in biological samples [43]. The relationship between the ethanol concentration in water and the corresponding ε_r of the solution is reported in [44] and [45].

During the whole experimental activity, the solution volume is maintained constant at 2 cm^3. Whenever the ethanol volume fraction is varied, a good alignment between the resonator and the vial is ensured by means of some references drawn on the substrate to improve the measurement repeatability. The S-parameters are acquired for each test with the Agilent 8753ES VNA. It is set to acquire 1601 points in the frequency range from 2 to 3 GHz, with an intermediate frequency (IF) bandwidth of 1 kHz. A full two-port coaxial short-open-load-thru (SOLT) calibration is performed on the VNA before the measurement session.

The magnitude of the measured S_{21} parameter at different ethanol volume fractions is reported in Fig. 8. The two resonant peaks clearly show a shift in frequency as well as

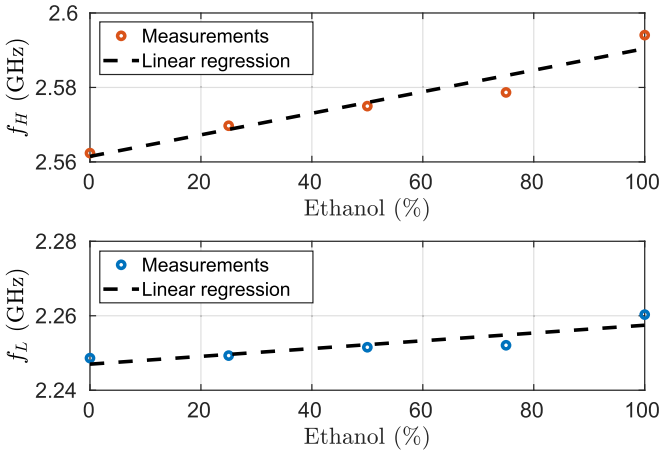

Fig. 9. Behavior of f_L and f_H as a function of the ethanol volume fraction: measurements (circles) and linear fitting (lines). The best fitting assumed linear is characterized by $R^2 = 0.71$ for f_L and $R^2 = 0.91$ for f_H.

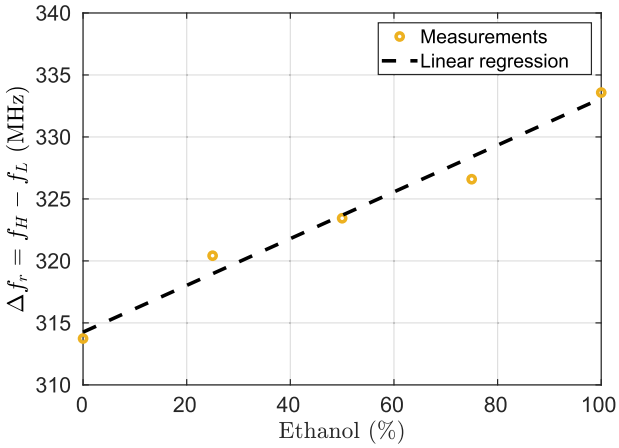

Fig. 10. Behavior of the frequency separation (Δfr) between the two resonant peaks as a function of the ethanol concentration: measurements (orange circles) and linear fitting (dashed black lines). The best fitting assumed linear is characterized by $R^2 = 0.97$.

a change in amplitude. It is worth noting that one resonant peak has a larger sensitivity to the ethanol concentration than the other, as described previously in Section II.

VI. Results and Discussion

The two resonant frequencies and the Q-factors are derived from the measured S-parameters by means of the extraction procedure described in Section IV. The estimated values of f_L and f_H are plotted in Fig. 9 as a function of the ethanol volume fraction. The frequency f_L is characterized by a sensitivity of 105 kHz/%ethanol, estimated from a linear regression model ($R^2 = 0.71$), whereas f_H exhibits a sensitivity of 290 kHz/%ethanol ($R^2 = 0.91$), which is almost three times higher. The frequency separation $\Delta f_r = f_H - f_L$ is plotted in Fig. 10. In this case, the linearity is improved with an $R^2 = 0.97$ and a sensitivity of 188 kHz/%ethanol. The limit of detection (LOD) has been estimated using the following equation [46]:

$$\text{LOD} = 3.3 \cdot \frac{\text{RSD}}{S} \tag{9}$$

where RSD is the residual standard deviation of the linear regression and S represents the device sensitivity. This calculation resulted in an LOD of 21% of ethanol. This value may be further reduced by improving the experimental reproducibility of the test, for example, by ensuring consistent vial positioning and accurate preparation of the water/ethanol mixture. It is worth noting that using only f_H as a tracker for the ethanol volume fraction instead of Δf results in a higher LOD (i.e., 34% of ethanol), further demonstrating the improved performance of the sensor using the differential approach. The main benefit of using Δf_r rather than f_H or f_L as the tracker for ε_r measurement is that common mode disturbance and other effects that could affect the measurement of both f_L and f_H (such as calibration problems and environmental temperature drift) can be reduced by considering the difference between the two resonant frequencies.

The Q-factors of the two resonant peaks are shown in Fig. 11. They exhibit a monotonic trend with the increase

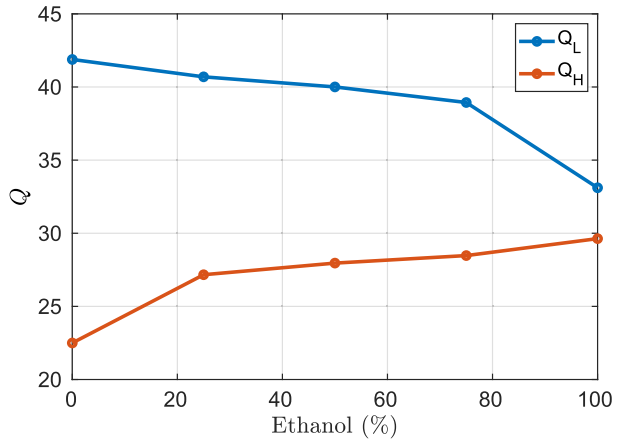

Fig. 11. Quality factor of the resonant peaks: Q_L at 2.30 GHz and Q_H at 2.62 GHz as a function of the ethanol volume fraction.

in the ethanol volume fraction in water; in particular, Q_L decreases, whereas Q_H increases.

In general, comparing the performance of sensors with different topologies, materials, and operating frequencies is not a straightforward task. However, for the purpose of providing a general overview of the state-of-the-art, Table I presents a comparative overview of the performance of the proposed sensor with other similar sensors that have been reported in the literature for investigating water/ethanol mixtures. The relationship between the resonant frequency and the ethanol volume fraction can be reasonably considered linear with a good approximation for all the sensors reported in the table. The proposed sensor exhibits a sensitivity value that is consistent with those reported in the table; however, this value is slightly lower than those of the other sensors. This can be attributed to the fact that the sensor has been fabricated using a low-cost technique (i.e., IJP) and a low-cost substrate (i.e., FR4 with $\varepsilon_r = 4.8$ and $\tan\delta = 0.02$). In addition, the proposed sensor is designed to be used for contactless measurements, specifically for the dielectric characterization of liquids inside a container (e.g., a Petri dish), and, then, the distance (or the container thickness) may be the inherent reason for the reduced

TABLE I
COMPARISON WITH OTHER MICROWAVE SENSORS

Ref.	f_0 (GHz)	Resonator Topology	Substrate	Size (mm^2)	Differential	Sensitivity (kHz/%ethanol)	Contactless
[47]	0.8 – 0.95	SRR	Rogers RO3010	86 × 62	Yes	500	No
[48]	2.4	CSRR	Rogers RO3035	20 × 28	No	450	Yes
[49]	2.45	Dielectric	FR4/Zirconia	120 × 80	No	718	No
[50]	2.4	Spiral resonators	Rogers RO4003C	15 × 20	No	2970	Yes
[51]	2.0	SRR	RT/duroid 6010.2LM	$\sim$ 30 × 30	No	$\sim$ 1000	No
This work	2.2 - 2.6	Coupled SRRs	FR4	60 × 20	Yes	188	Yes

sensor sensitivity. By using low-loss microwave dielectric substrates or by minimizing the distance between the sensor and the material under test, it might be possible to further improve the sensitivity of the developed sensor. However, despite this, the proposed sensor still exhibits a good level of performance and its low-cost fabrication technique and contactless measurement approach make it a cost-effective and attractive solution for the dielectric characterization.

The study has been extended considering the relative change of the capacitive contribution associated with the two resonances. Each resonance is characterized by an inductive and capacitive contribution. Considering that, in the first approximation, the inductance depends mainly on the geometrical parameters of the microwave resonator, it can be considered constant with respect to the ethanol concentration. Let C_{L_0} be the capacitive contribution of the first resonance at 0% ethanol (i.e., the reference), and let C_{L_E} be the capacitive contribution at a generic ethanol concentration. Then, the resonant frequency f_L has two different expressions

$$f_{L_0} = \frac{1}{2\pi\sqrt{\mathrm{L}C_{L_0}}} \tag{10}$$

at 0% ethanol and

$$f_{L_E} = \frac{1}{2\pi\sqrt{\mathrm{L}C_{L_E}}} \tag{11}$$

at any other ethanol volume fraction. Similarly, f_H can be expressed as

$$f_{H_0} = \frac{1}{2\pi\sqrt{\mathrm{L}C_{H_0}}} \tag{12}$$

$$f_{H_E} = \frac{1}{2\pi\sqrt{\mathrm{L}C_{H_E}}}. \tag{13}$$

From (10) and (11), the relative change in the capacitive contribution of the first resonance (f_L) is derived

$$\frac{C_{L_E}}{C_{L_0}} = \left(\frac{f_{L_0}}{f_{L_E}}\right)^2. \tag{14}$$

Similarly, from (12) and (13), it is possible to derive the capacitive contribution of the second resonance (f_H)

$$\frac{C_{H_E}}{C_{H_0}} = \left(\frac{f_{H_0}}{f_{H_E}}\right)^2. \tag{15}$$

The variation of these two relative capacitive contributions as a function of the ethanol concentration is shown in Fig. 12. As can be expected, since the inductive contribution has been considered constant and the two resonant frequencies are shifted toward higher frequencies as the ethanol concentration increases, the two capacitive contributions decrease with the ethanol concentration. Intuitively, this reduction of the capacitive effects associated with the two resonances might be ascribed to the decrease of ε_r when the ethanol concentration is increased. As a matter of fact, by increasing the ethanol concentration from 0% to 100%, ε_r decreases from 80.2 to 25.16.

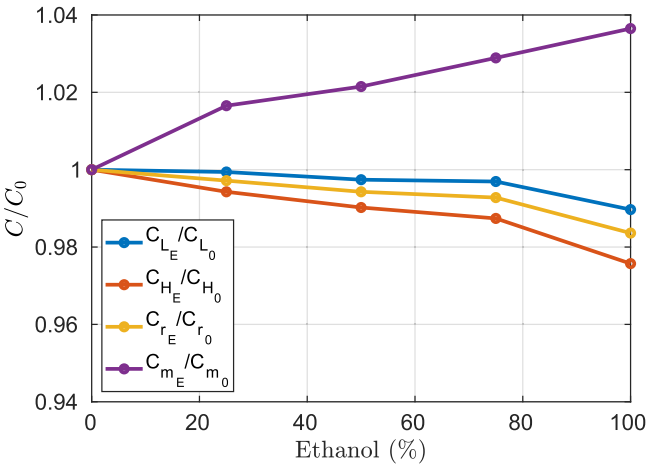

Fig. 12. Relative change with the ethanol variation of the capacitive contributions associated with the two resonances and the two capacitances C_r and C_m of the equivalent-circuit model.

As an alternative perspective, the achieved results can be analyzed by considering the two capacitances of the equivalent-circuit model shown in Fig. 2. Once again, the inductive contribution is here considered independent of the ethanol concentration. As done previously, f_L and f_H can be expressed in two different ways according to the ethanol content [33]

$$f_{L_0} = \frac{1}{2\pi\sqrt{L\left(C_{r_0} + C_{m_0}\right)}} \tag{16}$$

$$f_{L_E} = \frac{1}{2\pi\sqrt{L\left(C_{r_E} + C_{m_E}\right)}} \tag{17}$$

$$f_{H_0} = \frac{1}{2\pi\sqrt{L\left(C_{r_0} - C_{m_0}\right)}} \tag{18}$$

$$f_{H_E} = \frac{1}{2\pi\sqrt{L\left(C_{r_E} - C_{m_E}\right)}}. \tag{19}$$

From these equations, it is possible to derive straightforwardly the relative variation of C_r and C_m with the ethanol content

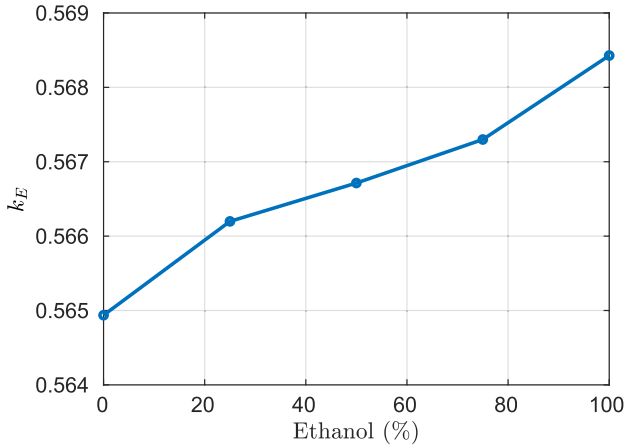

Fig. 13. Electric coupling coefficient between the two SRRs as a function of the ethanol volume fraction.

in the testing mixture

$$\frac{C_{r_E}}{C_{r_0}} = \frac{\frac{1}{f_{L_E}^2} + \frac{1}{f_{H_E}^2}}{\frac{1}{f_{L_0}^2} + \frac{1}{f_{H_0}^2}} \tag{20}$$

$$\frac{C_{m_E}}{C_{m_0}} = \frac{\frac{1}{f_{L_E}^2} - \frac{1}{f_{H_E}^2}}{\frac{1}{f_{L_0}^2} - \frac{1}{f_{H_0}^2}}. \tag{21}$$

The two quantities C_{r_E}/C_{r_0} and C_{m_E}/C_{m_0} are plotted in Fig. 12 as a function of the ethanol volume fraction. C_r decreases with increasing ethanol concentration. This decrease in C_r results in an increase in the two resonant frequencies, as can be clearly observed from (16)–(19) or their more general form in (2) and (3). On the other hand, the capacitance C_m, which represents the capacitive coupling between the two rings, increases as a result of the variation of the electrical coupling between the two resonant rings. It is worth noting that the relative variation of C_m is higher in comparison with the relative variations in the C_r capacitances. This is due to the position of the sample vial, which mainly affects the capacitive coupling between the two rings. Consequently, C_m can be considered the most representative sensing element of the equivalent-circuit model. This increase in C_m results in the increase in the frequency splitting Δf_r, as can be clearly observed from (16)–(19) or their more general form in (2) and (3). The variation of the electric coupling is the cause of the variation of the frequency splitting Δf_r. The electric coupling coefficient k_E between the two resonant rings can be calculated as [33]

$$k_E = \frac{f_H^2 - f_L^2}{f_H^2 + f_L^2}. \tag{22}$$

As shown in Fig. 13, k_E increases with the ethanol content in the mixture as the mutual capacitance C_m increases. As a result, the frequency separation Δf_r becomes wider.

VII. Conclusion

In this article, the development and validation of a differential two-port microwave sensor based on two capacitive coupled ring resonators have been presented and discussed. The sensor has been fabricated using IJP technology by depositing a silver-based conductive ink on an FR4 substrate. The validation procedure has been carried out by the extraction of the resonant parameters (i.e., resonant frequencies and Q-factors) from the behavior of the magnitude of S_{21} measured over the frequency range from 2 to 3 GHz and at different ε_r of the testing sample.

This is the first time that the structure based on two capacitive coupled SRRs has been successfully used for differential measurements. To accomplish this task, the separation between the two resonant frequencies occurring in the band from 2 to 3 GHz was used as the sensing parameter.

The study has been extended by considering the lumped-element equivalent-circuit model of the selected microwave resonator. This model provides a deeper understanding of the sensor behavior and its response to changes in the dielectric properties of the liquid under test. In particular, the relative change in the capacitances that contribute to the two resonances has been evaluated. It emerged that the electrical coupling between the two rings is affected by the ε_r of the mixture. By increasing the ethanol volume fraction in the solution, which implies a decrease in the effective ε_r, the mutual capacitance C_m increases, thus increasing the coupling coefficient. As a result, the frequency separation becomes higher. The described extraction procedure enabled a more accurate description of the sensor response, which is crucial for the design and optimization of the sensor and for the development of new sensing applications. Furthermore, the extraction of the relative change of the lumped-element values provides valuable information for future work on circuit design and optimization of the sensor.

In future work, the experimental validation will be extended by considering additional liquid mixtures and/or cell cultures for accomplishing their dielectric characterization, since the operation of the developed prototype is not limited to the considered samples, consisting of a variable mixture of ethanol and pure water at different volume ratios. Moreover, the effect of the parasitic capacitances on the sensing performance will be evaluated and minimized by investigating tailored design upgrades [52], [53].

References

[1] B. Andò, "Inkjet printing: A real opportunity for the next generation of low-cost sensors," *IEEE Trans. Instrum. Meas.*, vol. 16, no. 3, pp. 44–48, Jun. 2013.

[2] G. Gugliandolo, Z. Marinković, A. Quattrocchi, G. Crupi, and N. Donato, "Development of an inkjet-printed interdigitated device: CAD, fabrication, and testing," in *Proc. IEEE Int. Conf. Integr. Circuits, Technol. Appl. (ICTA)*, Nov. 2021, pp. 153–154.

[3] G. Gugliandolo et al., "Design and test of an inkjet-printed microwave interdigital capacitor on flexible Kapton substrate," in *Proc. 25th IMEKO TC-4 Int. Symp.*, Brescia, Italy, 2022, pp. 1–5.

[4] H. Lee, K. Naishadham, M. Tentzeris, and G. Shaker, "A novel highly-sensitive antenna-based 'smart skin' gas sensor utilizing carbon nanotubes and inkjet printing," in *Proc. IEEE Int. Symp. Antennas Propag. (APSURSI)*, Jul. 2011, pp. 1593–1596.

[5] B. Andò, S. Baglio, A. R. Bulsara, T. Emery, V. Marletta, and A. Pistorio, "Low-cost inkjet printing technology for the rapid prototyping of transducers," *Sensors*, vol. 17, no. 4, p. 748, 2017.

[6] K. Yan, J. Li, L. Pan, and Y. Shi, "Inkjet printing for flexible and wearable electronics," *APL Mater.*, vol. 8, no. 12, Dec. 2020, Art. no. 120705.

[7] G. Gugliandolo, G. Vermiglio, G. Cutroneo, G. Campobello, G. Crupi, and N. Donato, "Inkjet-printed capacitive coupled ring resonators aimed at the characterization of cell cultures," in *Proc. IEEE Int. Symp. Med. Meas. Appl. (MeMeA)*, Jun. 2022, pp. 1–5.

[8] S. P. Sreenilayam, I. U. Ahad, V. Nicolosi, V. A. Garzon, and D. Brabazon, "Advanced materials of printed wearables for physiological parameter monitoring," *Mater. Today*, vol. 32, pp. 147–177, Jan. 2020.

[9] M. Mass et al., "Fully inkjet-printed biosensors fabricated with a highly stable ink based on carbon nanotubes and enzyme-functionalized nanoparticles," *Nanomaterials*, vol. 11, no. 7, p. 1645, Jun. 2021.

[10] K. Crowley et al., "Fabrication of polyaniline-based gas sensors using piezoelectric inkjet and screen printing for the detection of hydrogen sulfide," *IEEE Sensors J.*, vol. 10, no. 9, pp. 1419–1426, Sep. 2010.

[11] J. Virtanen, L. Ukkonen, T. Björninen, A. Z. Elsherbeni, and L. Sydänheimo, "Inkjet-printed humidity sensor for passive UHF RFID systems," *IEEE Trans. Instrum. Meas.*, vol. 60, no. 8, pp. 2768–2777, Aug. 2011.

[12] R. Vyas et al., "Inkjet printed, self powered, wireless sensors for environmental, gas, and authentication-based sensing," *IEEE Sensors J.*, vol. 11, no. 12, pp. 3139–3152, Dec. 2011.

[13] G. Mattana et al., "Woven temperature and humidity sensors on flexible plastic substrates for E-textile applications," *IEEE Sensors J.*, vol. 13, no. 10, pp. 3901–3909, Oct. 2013.

[14] B. S. Cook, J. R. Cooper, and M. M. Tentzeris, "An inkjet-printed microfluidic RFID-enabled platform for wireless lab-on-chip applications," *IEEE Trans. Microw. Theory Techn.*, vol. 61, no. 12, pp. 4714–4723, Dec. 2013.

[15] A. Vena, L. Sydänheimo, M. M. Tentzeris, and L. Ukkonen, "A fully inkjet-printed wireless and chipless sensor for CO_2 and temperature detection," *IEEE Sensors J.*, vol. 15, no. 1, pp. 89–99, Jan. 2015.

[16] S. Cruz, D. Dias, J. C. Viana, and L. A. Rocha, "Inkjet printed pressure sensing platform for postural imbalance monitoring," *IEEE Trans. Instrum. Meas.*, vol. 64, no. 10, pp. 2813–2820, Oct. 2015.

[17] M. Bona, M. Serpelloni, E. Sardini, C. O. Lombardo, and B. Andò, "Telemetric technique for wireless strain measurement from an inkjet-printed resistive sensor," *IEEE Trans. Instrum. Meas.*, vol. 66, no. 4, pp. 583–591, Apr. 2017.

[18] A. Moya et al., "Online oxygen monitoring using integrated inkjet-printed sensors in a liver-on-a-chip system," *Lab Chip*, vol. 18, no. 14, pp. 2023–2035, 2018.

[19] D. Mojena-Medina, M. Hubl, M. Bäuscher, J. L. Jorcano, H.-D. Ngo, and P. Acedo, "Real-time impedance monitoring of epithelial cultures with inkjet-printed interdigitated-electrode sensors," *Sensors*, vol. 20, no. 19, p. 5711, Oct. 2020.

[20] S. Tonello, N. F. Lopomo, M. Serpelloni, M. Serzanti, P. Dell'Era, and E. Sardini, "Preliminary study of inkjet printed sensors for monitoring cell cultures," *Proc. Eng.*, vol. 168, pp. 578–581, Jan. 2016.

[21] L. Grob et al., "Inkjet-printed and electroplated 3D electrodes for recording extracellular signals in cell culture," *Sensors*, vol. 21, no. 12, p. 3981, Jun. 2021.

[22] N. Adly et al., "Printed microelectrode arrays on soft materials: From PDMS to hydrogels," *npj Flexible Electron.*, vol. 2, no. 1, pp. 1–9, May 2018.

[23] L. D'Alvia et al., "A novel microwave resonant sensor for measuring cancer cell line aggressiveness," *Sensors*, vol. 22, no. 12, p. 4383, Jun. 2022.

[24] J. C. Booth, N. D. Orloff, J. Mateu, M. Janezic, M. Rinehart, and J. A. Beall, "Quantitative permittivity measurements of nanoliter liquid volumes in microfluidic channels to 40 GHz," *IEEE Trans. Instrum. Meas.*, vol. 59, no. 12, pp. 3279–3288, Dec. 2010.

[25] X. Bao et al., "Integration of interdigitated electrodes in split-ring resonator for detecting liquid mixtures," *IEEE Trans. Microw. Theory Tech.*, vol. 68, no. 6, pp. 2080–2089, Jun. 2020.

[26] B. Xie et al., "High-sensitivity liquid dielectric characterization differential sensor by 1-bit coding DGS," *Sensors*, vol. 23, no. 1, p. 372, Dec. 2022.

[27] A. Ebrahimi, G. Beziuk, J. Scott, and K. Ghorbani, "Microwave differential frequency splitting sensor using magnetic-LC resonators," *Sensors*, vol. 20, no. 4, p. 1066, Feb. 2020.

[28] J. Bao, T. Markovic, G. Maenhout, I. Ocket, and B. Nauwelaers, "An impedance matched interdigital capacitor at 1.5 GHz for microfluidic sensing applications," *Sens. Actuators A, Phys.*, vol. 330, Oct. 2021, Art. no. 112867.

[29] C.-F. Liu, M.-H. Wang, and L.-S. Jang, "Microfluidics-based hairpin resonator biosensor for biological cell detection," *Sens. Actuators B, Chem.*, vol. 263, pp. 129–136, Jun. 2018.

[30] G. Gugliandolo, K. Naishadham, G. Neri, V. C. Fernicola, and N. Donato, "A novel sensor-integrated aperture coupled microwave patch resonator for humidity detection," *IEEE Trans. Instrum. Meas.*, vol. 70, pp. 1–11, 2021.

[31] M. H. Zarifi and M. Daneshmand, "Wide dynamic range microwave planar coupled ring resonator for sensing applications," *Appl. Phys. Lett.*, vol. 108, no. 23, Jun. 2016, Art. no. 232906.

[32] K. Luckasavitch, R. Kozak, K. Golovin, and M. H. Zarifi, "Magnetically coupled planar microwave resonators for real-time saltwater ice detection," *Sens. Actuators A, Phys.*, vol. 333, Jan. 2022, Art. no. 113245.

[33] J.-S. G. Hong and M. J. Lancaster, *Microstrip Filters for RF/Microwave Applications*. Hoboken, NJ, USA: Wiley, 2004.

[34] G. Gugliandolo, K. Naishadham, G. Crupi, G. Campobello, and N. Donato, "Microwave transducers for gas sensing: A challenging and promising new frontier," *IEEE Instrum. Meas. Mag.*, vol. 25, no. 3, pp. 42–51, May 2022.

[35] G. Gugliandolo, K. Naishadham, N. Donato, G. Neri, and V. Fernicola, "Sensor-integrated aperture coupled patch antenna," in *Proc. IEEE Int. Symp. Meas. Netw. (M&N)*, Jul. 2019, pp. 1–5.

[36] G. Gugliandolo, D. Aloisio, G. Campobello, G. Crupi, and N. Donato, "Development and metrological evaluation of a microstrip resonator for gas sensing applications," in *Proc. 24th IMEKO TC-4 Int. Symp.*, Palermo, Italy, 2020, pp. 14–16.

[37] Z. Marinković, G. Gugliandolo, M. Latino, G. Campobello, G. Crupi, and N. Donato, "Characterization and neural modeling of a microwave gas sensor for oxygen detection aimed at healthcare applications," *Sensors*, vol. 20, no. 24, p. 7150, Dec. 2020.

[38] C. Ramella, S. Corbellini, M. Pirola, L. Yu, and V. C. Fernicola, "Investigations on instability effects in a sapphire-based whispering gallery mode thermometer," in *Proc. IEEE Int. Instrum. Meas. Technol. Conf. (IMTC)*, May 2017, pp. 1–6.

[39] G. Gugliandolo, S. Tabandeh, L. Rosso, D. Smorgon, and V. Fernicola, "Whispering gallery mode resonators for precision temperature metrology applications," *Sensors*, vol. 21, no. 8, p. 2844, Apr. 2021.

[40] G. Gugliandolo, Z. Marinković, G. Campobello, G. Crupi, and N. Donato, "On the performance evaluation of commercial SAW resonators by means of a direct and reliable equivalent-circuit extraction," *Micromachines*, vol. 12, no. 3, p. 303, Mar. 2021.

[41] C. Ramella, M. Pirola, and S. Corbellini, "Accurate characterization of high-Q microwave resonances for metrology applications," *IEEE J. Microw.*, vol. 1, no. 2, pp. 610–624, Apr. 2021.

[42] A. P. Gregory and R. N. Clarke, "Traceable measurements of the static permittivity of dielectric reference liquids over the temperature range 5–50 °C," *Meas. Sci. Technol.*, vol. 16, no. 7, pp. 1506–1516, Jul. 2005.

[43] M. Hussein, F. Awwad, D. Jithin, H. El Hasasna, K. Athamneh, and R. Iratni, "Breast cancer cells exhibits specific dielectric signature in vitro using the open-ended coaxial probe technique from 200 MHz to 13.6 GHz," *Sci. Rep.*, vol. 9, no. 1, pp. 1–8, Mar. 2019.

[44] J. Wyman, "The dielectric constant of mixtures of ethyl alcohol and water from −5 to 40°," *J. Amer. Chem. Soc.*, vol. 53, no. 9, pp. 3292–3301, 1931.

[45] P. Petong, R. Pottel, and U. Kaatze, "Water–Ethanol mixtures at different compositions and temperatures. A dieletric relaxation study," *J. Phys. Chem. A*, vol. 104, no. 32, pp. 7420–7428, Aug. 2000.

[46] A. Shrivastava and V. B. Gupta, "Methods for the determination of limit of detection and limit of quantitation of the analytical methods," *Chronicles Young Scientists*, vol. 2, no. 1, pp. 21–25, Apr. 2011.

[47] P. Vélez, L. Su, K. Grenier, J. Mata-Contreras, D. Dubuc, and F. Martín, "Microwave microfluidic sensor based on a microstrip splitter/combiner configuration and split ring resonators (SRRs) for dielectric characterization of liquids," *IEEE Sensors J.*, vol. 17, no. 20, pp. 6589–6598, Oct. 2017.

[48] E. L. Chuma, Y. Iano, G. Fontgalland, and L. L. B. Roger, "Microwave sensor for liquid dielectric characterization based on metamaterial complementary split ring resonator," *IEEE Sensors J.*, vol. 18, no. 24, pp. 9978–9983, Dec. 2018.

[49] M. G. Mayani, F. J. Herraiz-Martínez, J. M. Domingo, R. Giannetti, and C. R.-M. García, "A novel dielectric resonator-based passive sensor for drop-volume binary mixtures classification," *IEEE Sensors J.*, vol. 21, no. 18, pp. 20156–20164, Sep. 2021.

[50] C. Gocen and M. Palandoken, "Machine learning assisted novel microwave sensor design for dielectric parameter characterization of Water–Ethanol mixture," *IEEE Sensors J.*, vol. 22, no. 3, pp. 2119–2127, Feb. 2022.

[51] W. Withayachumnankul, K. Jaruwongrungsee, A. Tuantranont, C. Fumeaux, and D. Abbott, "Metamaterial-based microfluidic sensor for dielectric characterization," *Sens. Actuators A, Phys.*, vol. 189, pp. 233–237, Jan. 2013.

[52] H. Abdelwahab, A. Ebrahimi, F. J. Tovar-Lopez, G. Beziuk, and K. Ghorbani, "Extremely sensitive microwave microfluidic dielectric sensor using a transmission line loaded with shunt LC resonators," *Sensors*, vol. 21, no. 20, p. 6811, Oct. 2021.

[53] A. Ebrahimi, J. Scott, and K. Ghorbani, "Ultrahigh-sensitivity microwave sensor for microfluidic complex permittivity measurement," *IEEE Trans. Microw. Theory Techn.*, vol. 67, no. 10, pp. 4269–4277, Oct. 2019.

Giovanni Gugliandolo (Member, IEEE) received the B.S. degree in electronic engineering and computer science and the M.S. degree in electronic engineering from The University of Messina, Messina, Italy, in 2013 and 2016, respectively, and the Ph.D. degree in metrology from the Politecnico di Torino, Turin, Italy, in 2020, in collaboration with the Istituto Nazionale di Ricerca Metrologica (INRiM).

In 2020, he joined The University of Messina, where he currently works with the Department of Engineering as an Assistant Professor in the field of electrical and electronic measurements. His research interests include sensors and sensor-based measurement systems, sensors metrology, and biomedical measurement systems.

Giovanna Vermiglio received the M.S. degree in medical biotechnology and the Ph.D. degree in science of receptor and posture from The University of Messina, Messina, Italy, in 2009, and 2013, respectively.

She is currently an Assistant Professor in histology and embryology with The University of Messina and also a member of the Laboratory of Histochemistry. She has coauthored more than 30 articles on international journals and conference proceedings (Scopus). Her current research interests include the involvement of several cell transmembrane proteins in cell–cell and cell–extracellular matrix/substrates interactions by optical and electron microscopy.

Giuseppina Cutroneo, photograph and biography not available at the time of publication.

Giuseppe Campobello (Member, IEEE) received the Laurea degree in electronic engineering and the Ph.D. degree in advanced technologies for information engineering from The University of Messina, Messina, Italy, in 2000 and 2004, respectively.

Since 2006, he has been with The University of Messina, where he is currently a Researcher and an Assistant Professor of telecommunications and the Head of the Laboratory of Wireless Communications. His current research interests include wireless sensor networks and signal processing techniques for telecommunications and biomedical applications.

Dr. Campobello is a member of the National Telecommunications and Information Technologies Group (GTTI) and the Microwave Engineering Center for Space Applications (MECSA).

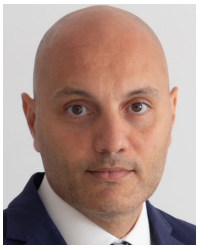

Giovanni Crupi (Senior Member, IEEE) is currently an Associate Professor with The University of Messina, Messina, Italy. His main research interests include the characterization and modeling of microwave transistors for wireless applications, as well as that of microwave sensors for bioengineering applications.

Dr. Crupi is an Editor-in-Chief of the *International Journal of Numerical Modelling: Electronic Networks, Devices and Fields* (Wiley), a Section Editor-in-Chief of the *Electronics* (MDPI), and also an Associate Editor of the journals IEEE MICROWAVE AND WIRELESS TECHNOLOGY LETTERS and IEEE ACCESS. He serves as a TPC Member for the IEEE INMMiC, TELSIKS, ICTA, and MMS conferences and also the TPC Chair for the IEEE INMMiC in 2014 and 2015. Since 2012, he has been the Chair of the IEEE MTT-S Graduate Fellowship Program.

Nicola Donato (Senior Member, IEEE) received the M.S. degree in electronic engineering from The University of Messina, Messina, Italy, in 1997, and the Ph.D. degree from the University of Palermo, Palermo, Italy, in 2002.

He is currently a Full Professor of electrical and electronic measurements with The University of Messina and the Head of the Laboratories of "Electronics for Sensors and for Systems of Transduction" and "Electrical and Electronic Measurements." He has coauthored more than 230 articles on international journals and conference proceedings (Scopus). His current research interests include sensor characterization and modeling, the development of measurement systems for sensors, and the characterization of electronic devices up to microwave range and down to cryogenic temperatures.

Open Access funding provided by 'Università degli Studi di Messina' within the CRUI CARE Agreement